

A Hybrid Surface Reference Technique and Its Application to the TRMM Precipitation Radar

R. MENEGHINI

NASA Goddard Space Flight Center, Greenbelt, Maryland

J. A. JONES

Science Systems and Applications, Inc., Lanham, Maryland

T. IGUCHI

National Institute of Information and Communications Technology, Tokyo, Japan

K. OKAMOTO

Osaka Prefecture University, Osaka, Japan

J. KWIATKOWSKI

George Mason University, Fairfax, Virginia

(Manuscript received 11 February 2004, in final form 26 May 2004)

ABSTRACT

Satellite weather radars that operate at attenuating wavelengths require an estimate of path attenuation to reconstruct the range profile of rainfall. One such method is the surface reference technique (SRT), by which attenuation is estimated as the difference between the surface cross section outside the rain and the apparent surface cross section measured in rain. This and the Hitschfeld–Bordan method are used operationally to estimate rain rate using data from the precipitation radar (PR) aboard the Tropical Rainfall Measuring Mission (TRMM) satellite. To overcome some of the problems associated with the latest operational version of the SRT, a hybrid surface reference is defined that uses information from the along-track and cross-track variations of the surface cross sections in rain-free areas. Over ocean, this approach eliminates most of the discontinuities in the path-attenuation field. Self-consistency of the estimates is tested by processing the orbits backward as well as forward. Calculations from 2 weeks of PR data show that 90% of the rain events over ocean for which the SRT is classified as reliable or marginally reliable are such that the absolute difference between the forward and backward estimates is less than 1 dB.

1. Introduction

A critical element in estimating rain rate from high-frequency radars is the determination of the path-integrated attenuation (PIA) along the radar beam. For a spaceborne radar this is tantamount to estimating the attenuation along the radar beam from the top of the atmosphere to the surface. For a single-wavelength radar, three methods have been used for this purpose: the Hitschfeld–Bordan (1954) method (HB), the surface reference technique (SRT), and the mirror image. The mirror-image return is of limited utility as an operational

algorithm for the Tropical Rainfall Measuring Mission (TRMM) precipitation radar (PR) because it is usually detectable only over the ocean at moderate rainfall rates (Li and Nakamura 2002; Liao et al. 1999). Moreover, the retrieval methods so far proposed are relevant only to near-nadir incidence. Although the HB estimate tends to become unstable in the presence of high attenuation, the approach provides useful corrections at light to moderate rain rates at Ku-band frequencies for a well-calibrated radar such as the PR. In practice, the operational rain-rate algorithm uses information from the HB and the SRT with a weighting based on the reliability of the estimates (Iguchi et al. 2000).

Description of the operational SRT algorithm was given by Meneghini et al. (2000) based on earlier work (Meneghini et al. 1983, 1987). An alternative approach

Corresponding author address: Dr. Robert Meneghini, NASA Goddard Space Flight Center, Code 975, Greenbelt, MD 20771.
E-mail: bob@neptune.gsfc.nasa.gov

was proposed by Li et al. (2002), who first determine the wind field based on the rain-free surface cross sections and then employ a model function to convert the wind field to surface cross sections, which are then taken as the reference data. The authors show that this procedure eliminates discontinuities in the PIA field that are sometimes seen in the operational results. Durden et al. (2003), using data from the Ku-band Airborne Mapping Radar (ARMAR), devised and applied an upgrade of the method using Doppler-derived wind speed and wind direction information. Quartley et al. (1999) have described a version of the method for application to the Ocean Surface Topography Experiment (TOPEX) altimetry data. Despite its nadir-viewing geometry and lack of direct rain backscatter, TOPEX provides normalized surface cross sections at both Ku- and C-bands so that a dual-wavelength version of the method is applicable. There have been a number of studies of the method using airborne radar data (e.g., Meneghini et al. 1989; Marzoug and Amayenc 1994; Iguchi and Meneghini 1994; Marecal et al. 1997; Durden and Haddad 1998). Recently, Tian et al. (2002) have applied the SRT over land to 10-GHz airborne radar data, showing that while the scattering cross sections are highly variable at nadir, the surface can serve as a stable reference at an incidence angle of 30° . Using the National Aeronautics and Space Administration (NASA) scanning radar altimeter (SRA) operating at 36 GHz, Walsh et al. (2002) measured the normalized radar cross section of the surface over a range of near-nadir incidence angles. From these data the average rain rate and the average sea surface mean square slope over the approximately 1.5-km swath of the instrument can be derived. While most studies have been carried out over the frequency range 10–36 GHz, the approach has been applied to 94-GHz airborne radar data (Li et al. 2001) and has been considered as a potential technique for analyzing data from a spaceborne cloud radar (L'Ecuyer and Stephens 2002).

The objective of the paper is to describe the latest version (version 6) of the TRMM PR algorithm 2a21 used to estimate the PIA. We focus on a description of a hybrid surface reference over ocean and the use of forward and backward processing of the data to assess the self-consistency of the estimates. An advantage of the present approach over the previous operational version (version 5) is that it largely eliminates discontinuities in the estimated PIA field over water backgrounds. As it is based on the requirement that the PIA be determined “on the fly,” in that reference data are taken only from prior scans, it differs from the model-function approach of Li et al. (2002). It also differs from the Li et al. approach in that a conversion to a wind field is not employed as an intermediate step in the estimation of the surface reference.

Sections 2 and 3 describe the method and provide definitions of several reference datasets. Examples of

the retrievals and statistical comparisons of the forward and backward results are given in section 4.

2. Description of the method

If we were able to measure the normalized radar cross section (NRCS) of the surface with the atmosphere in states a_1 and a_2 , the difference between the measurements would be equal to the difference in the path-integrated attenuations between a_1 and a_2 along the radar beam. If a_1 is free of precipitation and a_2 contains precipitation then the measured difference can be ascribed to the path attenuation by precipitation. Explicitly, if $\sigma^0(a_1)$, $\sigma^0(a_2)$ are the apparent NRCSs (in dB) measured at the surface under atmospheric conditions a_1 and a_2 , then the two-way path attenuation (in dB) can be estimated from the difference $\sigma^0(a_1) - \sigma^0(a_2)$. This is the basic approach used in the SRT. As an estimate of attenuation by precipitation, there are a number of sources of error associated with it.

- 1) In practice, the backscattered power cannot be measured from the same patch of surface with the atmosphere in two states. We can either measure the surface return at approximately the same location at a different time, before or after the rain event, or at approximately the same time but at different locations, preferably at the same incidence angle near the rain area.
- 2) Ice and water clouds, water vapor, and other gases introduce attenuation. These effects can be ignored only if they are the same for a_1 and a_2 or if the total attenuation in both cases is much less than the attenuation from the precipitation. If neither assumption holds, then the measured difference will have a term proportional to the differential attenuation between a_1 and a_2 caused by differences in cloud water and ice and gaseous attenuations between the two states.
- 3) Backscattered power from the rain will arrive at the receiver at the same time as the surface return. The amount of the rain return relative to the total return power depends on the rain rate, surface cross section, incidence angle, transmitted pulse width, and antenna beamwidth.
- 4) In the presence of very high rain rates, the surface return will fall below the noise level. The magnitude of the rain-free reference surface cross section (dB), relative to the noise, provides a lower bound to the actual path attenuation.
- 5) The surface return is estimated on the basis of 64 radar samples (Kozu et al. 2001). Assuming that they are independent and that the target is Rayleigh, consisting of a large collection of independent scattering facets, the standard deviation of the estimate, using logarithmic detection, is $5.57/\sqrt{64}$, or 0.7 dB. It follows that the standard deviation of the path-attenuation estimate must be at least this large.

6) A problem with the assumption that the surface cross sections are the same outside and within the rain is the influence of the rain itself on the surface cross section. This effect over ocean depends on rain rate, radar incidence angle, and wind speed (Bliven and Giovanangeli 1993; Yang et al. 1997). However, even if a functional form for these effects were available, we would need to estimate the rain rate and wind speed and apply the correction in an iterative fashion.

In this paper, we assess the reliability of the PIA estimates by considering different surface reference datasets and by processing the orbits backward as well as forward to test the self-consistency of the estimates. To some extent, this helps quantify the first two error sources. Because of the narrow beamwidth of the PR (0.71°) and its near-nadir scanning, the third source of error usually can be neglected. Although cases can be found where the signal attenuation is sufficiently strong to mask the surface return, these occurrences are rare and this source of error usually can be neglected. Of course, with the use of a higher-frequency radar, such as Ka band, the loss of the surface return will occur more frequently. Determining the influence of rain on the surface cross section requires further experiment. Some indication of its effect on the accuracy of the PIA may be possible by comparing several methods of attenuation estimation that depend in different ways, or not at all, on the surface scattering properties. To isolate and compare the separate sources of error in the various approaches is a formidable task, however, and beyond the scope of the paper.

3. Surface reference estimates

a. Temporal reference

The PR cross-track scan covers a swath of approximately 220 km and consists of data from 49 incidence angles: $0^\circ, \pm 0.75^\circ, \pm 1.5^\circ, \dots, \pm 18^\circ$, where “ \pm ” indicates that for a nominal spacecraft attitude, the set of angles on the right- and left-hand sides of the swath are the same. Grouping the data according to incidence angle, irrespective of sign, gives 25 distinct angles.

Assume that a range–reflectivity profile is measured in the presence of rain at location L at an incidence angle θ at time t . As already noted, there are two principal ways to obtain a surface reference measurement: measure the NRCS at (L, θ) but at an earlier or later time under rain-free conditions or measure the NRCS at approximately the same time at a nearby rain-free location, L' . We refer to the first type of measurement as a temporal reference (same location as the rain event but at a different time) and the second type as a spatial reference (different location but at approximately the same time).

To obtain a temporal reference dataset, a $1^\circ \times 1^\circ$ latitude–longitude grid is defined that extends from 36°S

to 36°N . For each grid cell the sample mean, $\sigma_T^0(\text{NR}, |\theta_j|)$, and standard deviation, $S_T(\text{NR}, |\theta_j|)$ (dB), of the NRCS, under nonraining conditions (NR) are calculated for each of the 25 incidence angles of the PR. For a measurement of the apparent cross section, $\sigma^0(R, \theta_j)$, made in the presence of rain (R) at angle θ_j ($j = 1, \dots, 49$) the two-way path-integrated attenuation (dB) is estimated from

$$A_T(\theta_j) = \sigma_T^0(\text{NR}, |\theta_j|) - \sigma^0(R, \theta_j). \quad (1)$$

The reliability, Rel , of the estimate is defined by

$$\text{Rel}_T = A_T(\theta_j)/S_T(\text{NR}, |\theta_j|). \quad (2)$$

In the operational version of the algorithm, the temporal reference dataset is updated each month. For example, the temporal reference data for the month of June 1998 are computed from rain-free surface cross sections taken during the month of May 1998.

b. Spatial reference

Three types of spatial reference data are discussed: along track, cross track, and hybrid. In contrast to the categorization of the temporal reference data, where the sign of the angle, designating the left- and right-hand sides of the swath, is ignored, for the spatial reference the 49 angle bins are treated separately. Note also that separate spatial reference sets are made for each of the three surface types: ocean, coast, and land, where the background is categorized as coast when land and ocean are judged to be present within the same field of view.

The along-track reference data are obtained by calculating the sample mean and standard deviation of the NRCS over the last k rain-free fields of view prior to the detection of rain. In the present code $k = 8$. These reference fields are computed independently for each of the 49 incidence angles so that if rain is detected at cross-track scan N at angle θ_j , the normalized surface cross sections from the last k rain-free fields of view at angle θ_j are used to estimate the mean and standard deviation of the along-track surface reference. Using “AS” to denote the along-track spatial reference, the sample mean and standard deviation are written $\sigma_{\text{AS}}(\text{NR}, \theta_j)$ and $S_{\text{AS}}(\text{NR}, \theta_j)$, respectively. The estimated PIA and associated reliability are given by the equations

$$A_{\text{AS}}(\theta_j) = \sigma_{\text{AS}}^0(\text{NR}, \theta_j) - \sigma^0(R, \theta_j), \quad (3)$$

$$\text{Rel}_{\text{AS}} = A_{\text{AS}}(\theta_j)/S_{\text{AS}}(\text{NR}, \theta_j). \quad (4)$$

The reliability definitions given by (2) and (4) are equal to the inverse of the fractional standard deviation of the estimate. One of the goals of the paper is to assess this measure of reliability relative to that derived from processing the data in the forward and backward directions.

A schematic of the selection process for the surface reference datasets is shown in Fig. 1, where the cross-hatched area represents rain. To estimate the PIA at the field of view (FOV) located at scan N and incidence

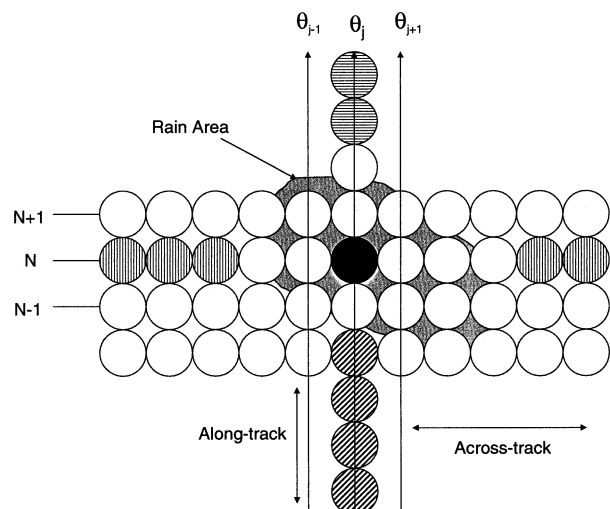


FIG. 1. Schematic of the selection method of surface scattering cross sections for along-track and cross-track reference data for determination of path attenuation at the FOV (in black). Along-track reference data for forward processing are shown by the diagonally hatched FOVs and for backward processing by the horizontally hatched FOVs. Cross-track reference data are taken from FOVs with vertical hatching.

angle θ_j shown in black, we first calculate the mean and standard deviation from prior rain-free fields of view at the same incidence angle. The fields of view from which a portion of the along-track reference data would be taken are represented in the figure by the four diagonally hatched circles. If the orbit were run backward, with the last scan of the orbit processed first, then a portion of the along-track reference data would be taken to be those rain-free fields of view shown near the top of the figure with horizontal hatching. Since the reference data will be different in the two cases so will the estimated path attenuations.

Figure 1 also shows a portion of the fields of view that would be used for the cross-track spatial reference, represented in the diagram by the circles with vertical hatching. Unlike the along-track reference, where the incidence angle is fixed and the reference is simply the sample mean of the rain-free NRCS, for the cross-track reference an account must be made for the angular variation in σ^0 . Assuming that the angular variation of the ocean surface cross section can be modeled as a quadratic, then

$$\sigma_{\text{XS}}^0(a, b, c; \theta) = a\theta^2 + b\theta + c. \quad (5)$$

[The expression $\sigma^0 = a\theta^2 + c$ follows as a small angle approximation to the standard physical optics expression for σ^0 (e.g., Freilich and Vanhoff 2003); the term $b\theta$ provides for a possible asymmetry between the right- and left-hand sides of the swath caused by the wind direction or uniform changes in the wind speed.] Data from the rain-free portions of the cross-track scan can be used to estimate the coefficients, a , b , and c , by minimizing the mean square error between the fit and

the data. Once this is done, the two-way PIA at angle θ_j within the scan is estimated from

$$A_{\text{XS}}(\theta_j) = \sigma_{\text{XS}}^0(a, b, c; \theta_j) - \sigma^0(R, \theta_j). \quad (6)$$

By analogy to the other cases, the reliability of the estimate is defined by

$$\text{Rel} = A_{\text{XS}}(\theta_j)/S_{\text{XS}}, \quad (7)$$

where S_{XS} is the rms difference between the fitting function (5) and the rain-free data within the scan.

Both the spatial and temporal references are deficient in certain respects. For example, the estimated PIA field sometimes shows streaks that result from the path attenuations along one or more angles that are higher or lower than those in adjacent angles. Although these discontinuities often arise from a mixing of spatial and temporal reference data, they also occur when the along-track reference is used exclusively. The cross-track reference suffers from the problem that the number of rain-free reference data points varies from scan to scan. In cases where rain fills most or all the swath (220 km) the coefficients in the fitting function are either unreliable or indeterminate. To circumvent these deficiencies, we use a combination of the two approaches as described below.

At each scan, the mean and standard deviation of the along-track reference data are available at each of the 49 angles. These data, which characterize the behavior of prior rain-free surface cross sections, can be used to calculate the coefficients of a cross-track quadratic fit with weights that are inversely proportional to the standard deviation $S_{\text{AS}}(\text{NR}, \theta_j)$ of the along-track estimates. Specifically, the problem is to find the coefficients a , b , and c of the quadratic that minimize the function, F :

$$F = \sum_{j=1}^{49} \frac{[\sigma_{\text{AS}}^0(\text{NR}, \theta_j) - \sigma_{\text{XS}}^0(a, b, c; \theta_j)]^2}{S_{\text{AS}}(\text{NR}, \theta_j)}, \quad (8)$$

where $\sigma_{\text{XS}}^0(\theta_j)$ is the model function given by (5) and $\sigma_{\text{AS}}^0(\text{NR}, \theta_j)$ is the mean along-track reference for the NRCS at θ_j . Once the coefficients are found, the PIA is estimated from the same formula used for the cross-track method:

$$A_{\text{HY}}(\theta_j) = \sigma_{\text{XS}}^0(a, b, c; \theta_j) - \sigma^0(R, \theta_j). \quad (9)$$

The reliability of the estimate is defined as

$$\text{Rel}_{\text{HY}} = \frac{A_{\text{HY}}(\theta_j)}{\left[\left(\frac{1}{49} \right) \sum_{j=1}^{49} S_{\text{AS}}^2(\text{NR}, \theta_j) \right]^{1/2}}. \quad (10)$$

In version 5 of the operational algorithm a global reference is defined in a similar way to the temporal reference. However, unlike the temporal reference, where the mean and standard deviation are computed over $1^\circ \times 1^\circ$ latitude-longitude bins for the 25 incidence angles, the global is computed from all rain-free data, separated by background type and incidence angle but not by location. For example, over land we can write

the 25 mean reference values and associated standard deviations by $\sigma_{\text{gl,land}}^0(\text{NR}, |\theta_j|)$ and $S_{\text{gl,land}}(\text{NR}, |\theta_j|)$.

4. Results

a. Examples

The PIA field derived from 200 scans of the TRMM PR data is shown in Fig. 2. The data were taken from scans 1–200, orbit 24034 on 1 February 2002. A single scan of the PR sweeps out a rectangular area of approximately $4.3 \text{ km} \times 220 \text{ km}$, so that the spatial region displayed represents an area of approximately $860 \text{ km} \times 220 \text{ km}$ along the x and y axes, respectively. Shown in the top and center panels are the two-way path-integrated attenuations as estimated from the hybrid method; for the results in the top panel, the orbit is processed in the usual forward direction; for the results in the middle panel, the orbit is processed in reverse order. If the PIA is negative, the corresponding field of view is colored gray. In such cases the estimate is clearly unreliable and the attenuation is set to zero. The difference plot is shown in the bottom panel; if at a particular field of view the PIA is negative for either the forward or backward result, the element is colored gray.

To understand the general features of the difference plot, note that a rising wind speed reduces the near-nadir ($<10^\circ$) σ^0 values and increases the off-nadir ($>10^\circ$) values. These relationships are shown in Fig. 3, in which rain-free values of σ^0 from the PR are plotted versus the wind speed data from the QuikSCAT SeaWinds scatterometer (Lungu 2001; Draper and Long 2002) for incidence angles of 0° , 6° , 10.5° , 14.2° , and 18° . The data were obtained from measurements taken on a single day (7 September 1999) where the comparisons were made over $0.25^\circ \times 0.25^\circ$ latitude–longitude boxes. Similar scatterplots that relate TRMM PR measurements of σ^0 with wind speeds derived from the TRMM Microwave Imager (TMI) have been constructed (e.g., Li et al. 2002). The relationships show that if the winds are lower in the rain-free region preceding the rain than the winds encountered just after, then the surface reference values from the forward processing will be greater than those from the backward processing at near-nadir angles and smaller than those from the backward processing at off-nadir angles. This, in turn, will yield higher values of the PIA for the forward estimates at near-nadir incidence and lower values at off-nadir incidence. This behavior can be seen in the difference plot of Fig. 2 (bottom), over the rainband from scan 85 to 105. The opposite behavior occurs in the region from scan 110 to 160, where the path attenuations from the forward processing are less than those from the backward processing at near-nadir incidence and greater at off-nadir incidence.

The differences in the path attenuations estimated from forward and backward processing are consistent with the wind speed increasing from region 1 to region

2 and then decreasing from region 2 to region 3 (regions are labeled in the bottom panel of Fig. 2). For example, in the rainband from scan 85 to 105, the reference data for the backward processing are taken from the rain-free, “high wind” region 2, while the reference data for the forward processing are taken from the “low wind” region 1. For the rainband within scans 110 to 160, the reference data for the forward processing are now taken from the high-wind region 2, while the backward processing uses as reference the rain-free low-wind data from region 3.

Details of the estimation procedure at scan 100 are shown in Figs. 4 and 5 for the forward and backward estimates, respectively. The line at the bottom of each plot indicates the angles, within the scan, at which rain is detected. In the top panels of Figs. 4 and 5, the along-track reference data are displayed for all 49 angles, where the length of the vertical bar at each incidence angle θ_j is equal to twice the standard deviation, $2S_{\text{AS}}(\text{NR}, \theta_j)$, and where the midpoint is equal to the mean, $\sigma_{\text{AS}}^0(\text{NR}, \theta_j)$. The apparent normalized radar cross sections within the scan, $\sigma^0(R, \theta_j)$, are represented by the diamonds. The two-way along-track path-attenuation estimate, $A_{\text{AS}}(\theta_j)$, is equal to the difference between $\sigma_{\text{AS}}^0(\text{NR}, \theta_j)$ and $\sigma^0(R, \theta_j)$. This quantity is displayed in the bottom panel of Fig. 4 (gray line). As shown by (9), calculation of the PIA using the hybrid reference data, $\sigma_{\text{AS}}^0(\text{NR}, \theta_j)$, using as weighting functions the inverse of the standard deviation of the sample means, $S_{\text{AS}}(\text{NR}, \theta_j)$. The quadratic fit for this scan is represented in the top panel by the thick solid line. Denoting this by $\sigma_{\text{XS}}^0(a, b, c; \theta_j)$, the hybrid PIA is computed from (9) and is equal to the distance between the quadratic fit and the measured data $\sigma^0(R, \theta_j)$ at each θ_j . The results are displayed in the bottom panel (heavy solid line).

Shown in Fig. 5 is the same scan of data used in Fig. 4; that is, the apparent surface cross sections, represented by the diamonds, are the same in both cases. In this case, however, the reference data are taken from the backward-processed orbit. Path-attenuation estimates are shown in the lower panel for the hybrid and along-track reference data. For this scan, the differences between the forward and backward results are usually smaller if the hybrid reference is used. We will return to this issue in the next section, where the statistics are given for the forward–backward differences for both types of reference data.

An example of a well-organized tropical storm measured on 3 February 2002, orbit 24077, is shown in Fig. 6. As in Fig. 3, the forward and backward results using the hybrid reference are shown in the top and middle panels. The difference plot, shown at bottom, indicates that the forward and backward estimates of PIA for this case are usually within $\pm 1 \text{ dB}$ of each other. Details of the forward and backward estimates are shown in Figs. 7 and 8 using a scan where the path-attenuation estimates attain values in excess of 15 dB. For the forward

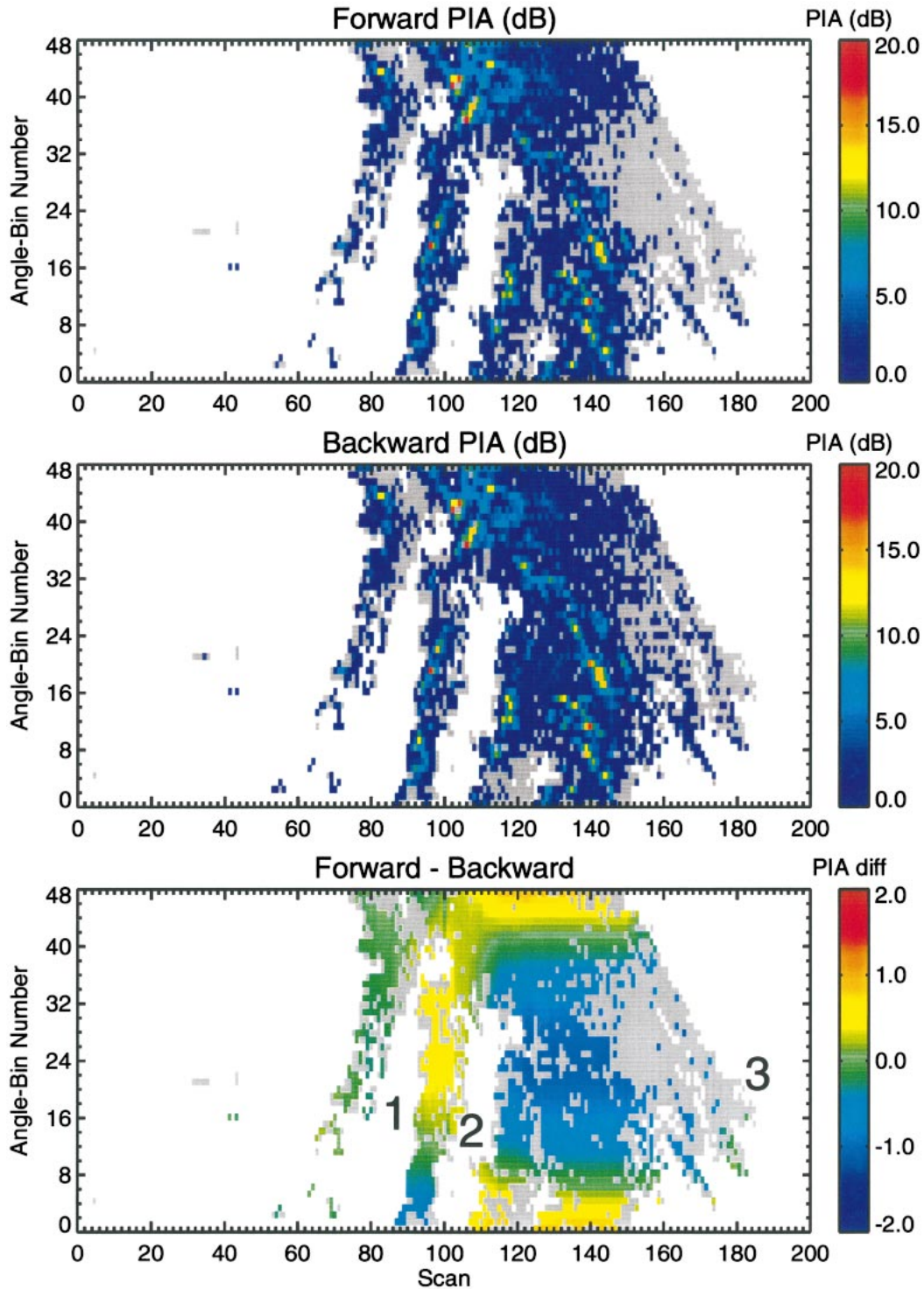


FIG. 2. Estimates of two-way path-integrated attenuation using the hybrid reference data for (top) forward and (middle) backward processing and (bottom) their difference for 200 scans of TRMM PR data measured on 1 Feb 2002, orbit 24034.

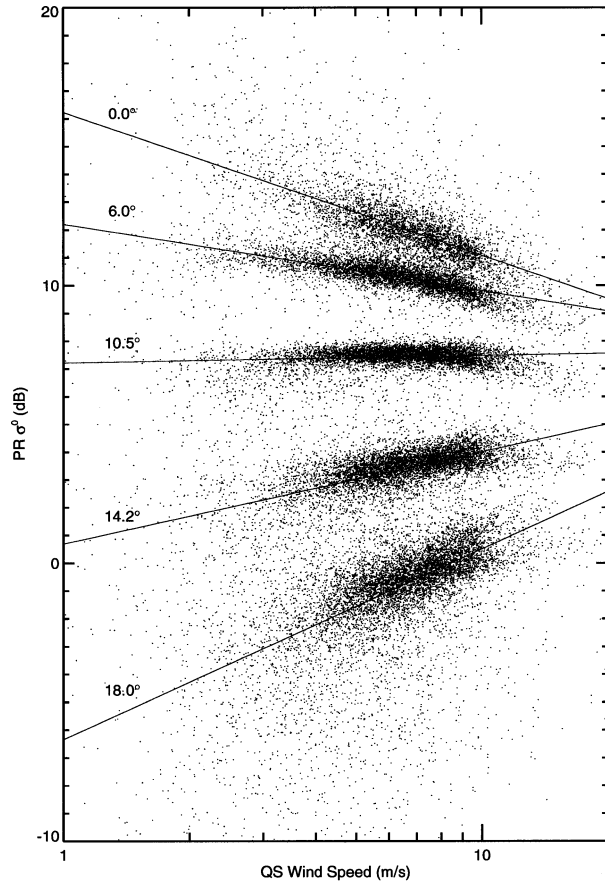


FIG. 3. Scatterplots of the normalized surface cross section, σ^0 , at five incidence angles as estimated from the TRMM PR data (ordinate) vs wind speed estimates from the SeaWinds scatterometer on the QuikSCAT satellite (QS).

processing, the quadratic fit passes near the mean values of the along-track estimates so that the hybrid and along-track PIA estimates are in good agreement. As seen in Fig. 8, the along-track estimates in the backward direction sometimes differ from the quadratic fit by more than 1 dB. Over large areas of rain such as this, where the reference data are not updated (since the hybrid and along-track reference datasets are updated only when rain-free regions are encountered), these high reference levels, particularly around -1° and 7° , tend to produce larger PIA estimates than adjacent angles and appear on the image as streaks. Because the quadratic fit tends to smooth out anomalous values, this problem occurs less often when the hybrid reference data are used.

Although the focus of the paper is the implementation of the hybrid method and evaluation of the SRT by forward and backward processing, it is necessary to point briefly to the differences between the versions 5 (v5) and 6 (v6) algorithms. For both algorithms, the standard deviation associated with the temporal reference, $S_T(\text{NR}, |\theta_j|)$, and along-track spatial reference, $S_{AS}(\text{NR}, \theta_j)$, are compared; if $S_{AS} < S_T$, then the along-track reference, $\sigma_{AS}^0(\text{NR}, \theta_j)$, is used in calculating the

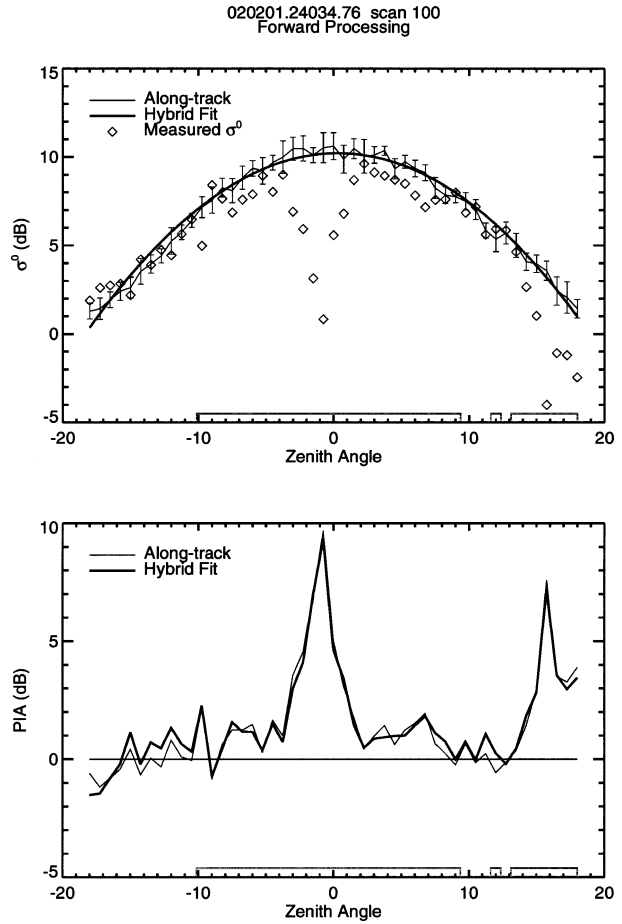


FIG. 4. (top) Diamonds represent apparent σ^0 values at scan 100. Mean and standard deviation of the along-track reference data are represented by the vertical bars. The quadratic fit through the data (heavy solid line) represents the hybrid reference curve. Line at bottom indicates the angles at which rain is detected. (bottom) Estimated two-way path-integrated attenuations as derived from the along-track and hybrid reference datasets.

PIA. Conversely, if $S_{AS} > S_T$, then the temporal reference, $\sigma_T^0(\text{NR}, |\theta_j|)$, is used. The associated reliability of the estimate is given by (2) or (4), depending on whether the temporal or along-track spatial reference is selected. Having chosen $\sigma_{AS}^0(\text{NR}, \theta_j)$ or $\sigma_T^0(\text{NR}, |\theta_j|)$ as the reference, say $\sigma_{\text{ref}}^0(\theta_j)$, a further test is made in v5 using the global reference data, $\sigma_{\text{gl}}^0(\theta_j)$. In particular, if $\sigma_{\text{ref}}^0 > \sigma_{\text{gl}}^0 + 2$ dB or $\sigma_{\text{ref}}^0 < \sigma_{\text{gl}}^0 - 2$ dB, then σ_{ref}^0 is replaced by σ_{gl}^0 and the associated standard deviation and reliability are replaced by S_{gl} and Rel_{gl} . In v6, the global reference has been eliminated while the hybrid reference has been introduced for swaths that are entirely over an ocean background. The selection of the reference data for v5 and v6 is shown in the flow diagram of Fig. 9.

Illustrated in the top panel of Fig. 10 are the v5 results for the same region used to display the hybrid PIA results in Fig. 6. (It should be noted that several other changes to the code have been made in going from v5

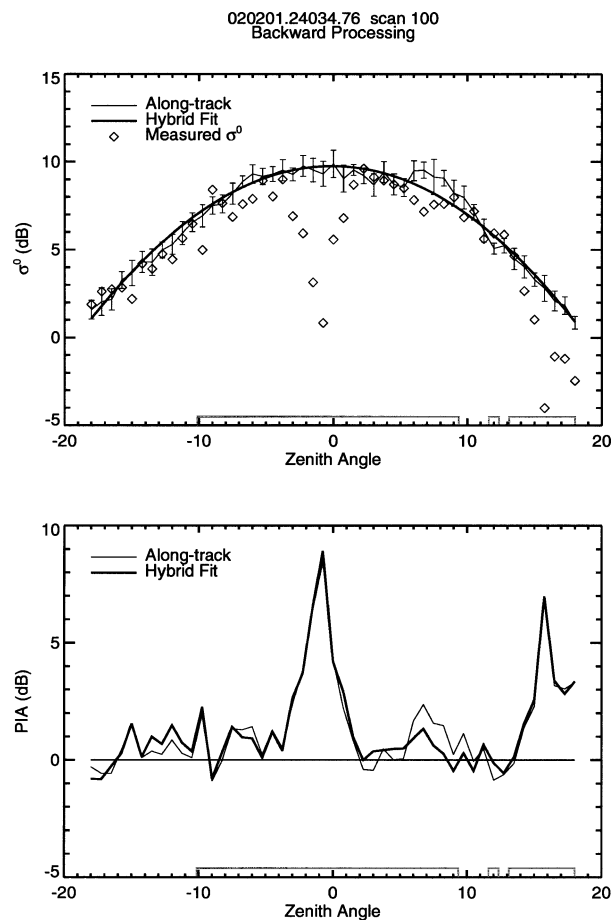


Fig. 5. Same as Fig. 4 but where the orbit is processed backward.

to v6 so that the v5 results shown here differ from the operational product. The main features of the results remain the same, however.) A difference plot of the v6 results from Fig. 6 (top panel), and v5 is shown in the center panel of Fig. 10. The discontinuities in the PIA evident in the upper panel can be explained primarily by the reference datasets used to compute the v5 path attenuation. These are shown in the lower panel, in which the raining areas using the along-track, temporal, and global reference data are depicted in blue, yellow, and red, respectively. Although the temporal dataset was intended primarily for land backgrounds, this reference occasionally has a smaller standard deviation than that associated with the along-track reference over ocean. Moreover, under high-wind conditions, the temporal or along-track reference is sometimes 2 dB lower than the global reference at near-nadir incidence and 2 dB higher at off-nadir incidence. As a result, the reference data can change frequently, as in this example, producing an estimated PIA field with discontinuities. (Because the global reference is used in less than 1% of the cases, this example is atypical.) Although the change in reference data appears to be the primary source of large irregularities in the PIA fields in v5, as was already

noted in connection with Fig. 8, discontinuities in the PIA field can arise even when the along-track reference data are used exclusively.

b. Statistics of PIA over ocean

A measure of the self-consistency of the estimates can be obtained by examining the histogram of differences between the path attenuations derived from forward and backward processing of the datasets. The statistics were compiled from a week of measurements in February 1998 and a week in February 2002, comprising 224 orbits of data. The difference is calculated only when both the forward and backward estimates have an associated reliability factor greater than unity. In particular, for the hybrid method, we require that the reliability factor defined by (10) be greater than unity. Of the 1 914 130 fields of view at which rain was detected over ocean during this 2-week period, 1 125 754 ($\cong 59\%$) of them were such that the PIA from the forward and backward estimates were both categorized as marginally reliable (where the reliability is between 1 and 3) or reliable (where the reliability is greater than 3). Of these, about 93% were calculated using the hybrid reference data. The other 7% occur when the background type in one or more fields of view within a scan are categorized as land or coast. The along-track surface reference accounts for 6.6% and the temporal 0.4% of the total. It is worth noting that whenever the hybrid is used for the forward processing, it is used for the backward processing as well. In contrast, when the hybrid is not used, the reference data may differ in the forward and backward directions; for example, the temporal may be used in the forward and the along-track spatial reference in the backward.

Letting A_F and A_B be the two-way path-integrated attenuation from the forward and backward directions, respectively, the histogram of the difference, $\delta A = A_F - A_B$, is shown in the top panel of Fig. 11. As noted above, only pairs of path attenuations (A_F, A_B) that have reliabilities greater than unity are used to construct the histogram. For the data shown in Fig. 11, 75% of the rain events are contained within the vertical solid lines at $\delta A = -0.46$ dB and $\delta A = 0.46$ dB; that is, in 75% of the cases, the absolute difference between the forward and backward path attenuations is less than 0.46 dB. Letting $\Pr[X]$ be the probability of X , this can be written

$$\{\Pr[|\delta A| < 0.46 \text{ dB}]\} = 0.75.$$

The dotted and dashed vertical lines shown in the plot define, respectively, the regions over which 90% and 95% of the data are contained, where

$$[\Pr(|\delta A| < 0.81 \text{ dB})] = 0.9,$$

$$[\Pr(|\delta A| < 1.12 \text{ dB})] = 0.95.$$

For example, 95% of the data classified as marginally reliable or reliable are such that the absolute difference

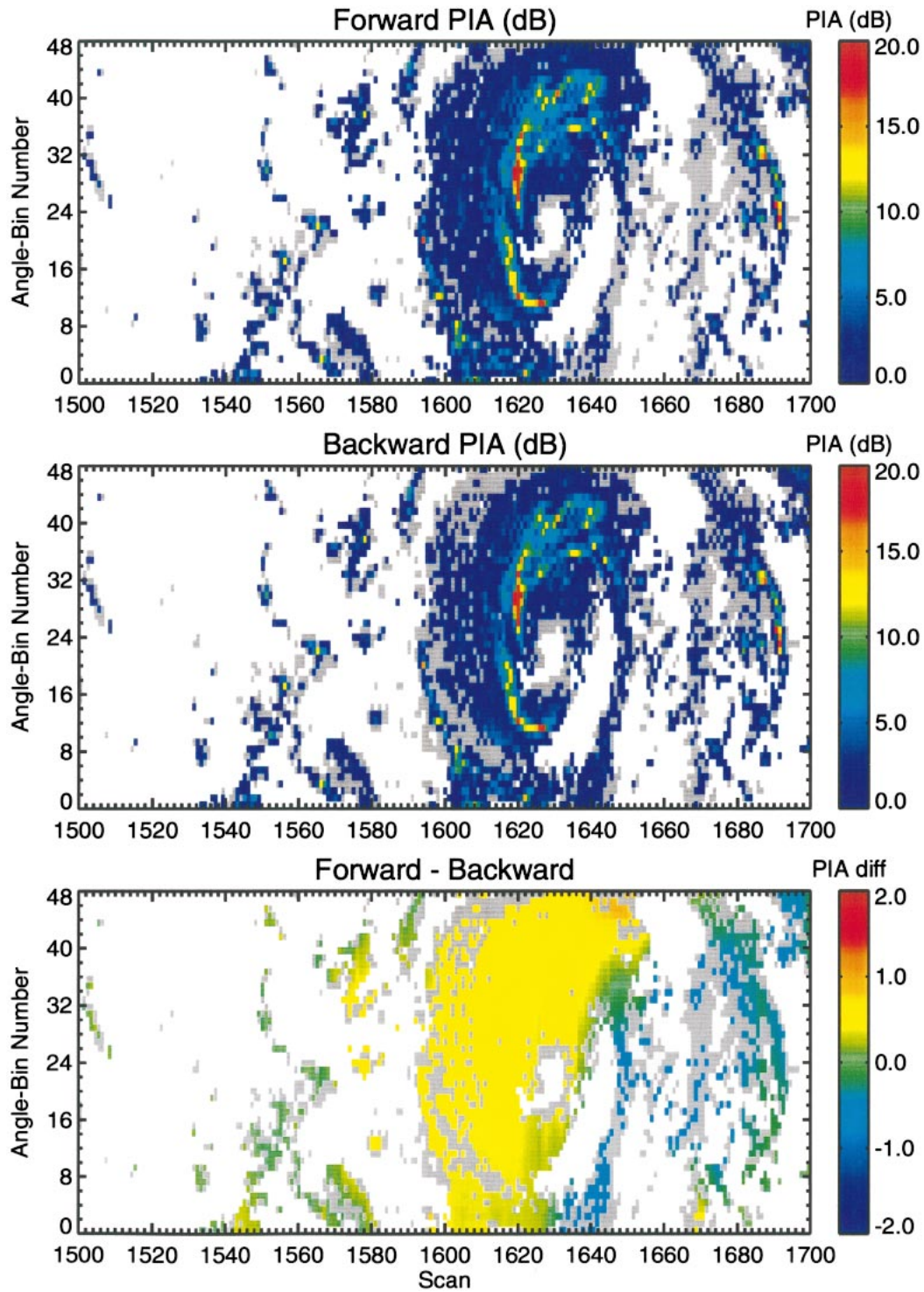


FIG. 6. Estimates of two-way path-integrated attenuation using the hybrid reference data for (top) forward and (middle) backward processing and (bottom) their difference for 200 scans of TRMM PR data measured on 3 Feb 2002, orbit 24077.

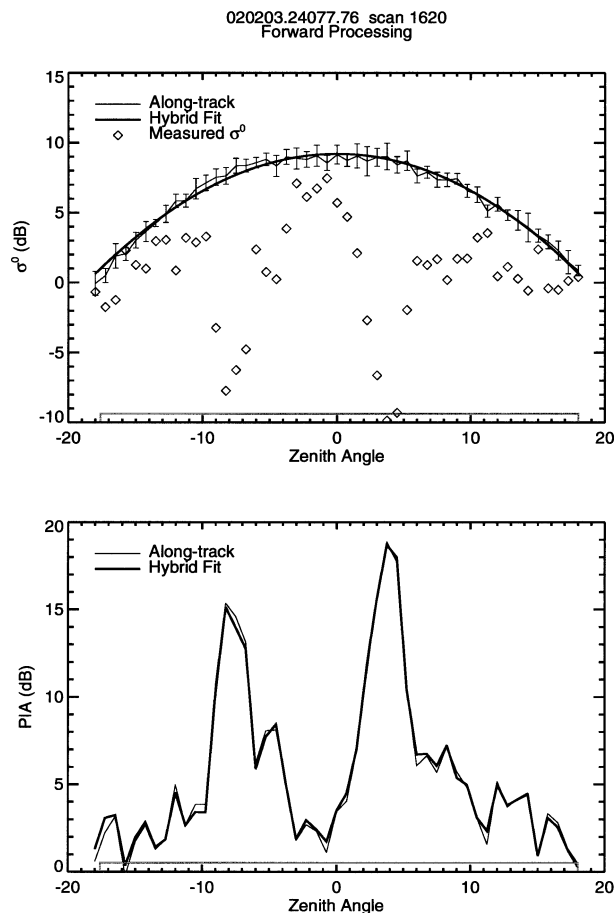


FIG. 7. Same as Fig. 4, but for scan 1620 of orbit 24077 measured on 3 Feb 2002.

between the backward and forward PIA estimates is less than 1.12 dB. To obtain a measure of the relative error, we plot in the bottom panel of Fig. 11 the histogram of the normalized quantity: $\delta A_N = \delta A / A_M = (A_F - A_B) / [0.5(A_F + A_B)]$. In this case we find that about 75% of the data have a relative error less than 25%; that is, the difference between the forward and backward estimates is less than a quarter of the average of these estimates 75% of the time. In 90% of the cases the difference is less than about 45% of the mean, and in 95% of the cases the difference is less than about 55% of the mean. The relative error can be reduced by imposing more stringent conditions on the data. For example, if we require that the reliability of both forward and backward estimates be 3 or greater, we find that 75% of the filtered data are within 10% of the mean and that 95% of the filtered data are within 30% of the mean. However, this improvement comes at the expense of excluding a much greater fraction of data. As noted above, if the reliability is required to be greater than unity for both the forward and backward PIA estimates, 41% of the rain data over ocean must be excluded; if the reliability of both esti-

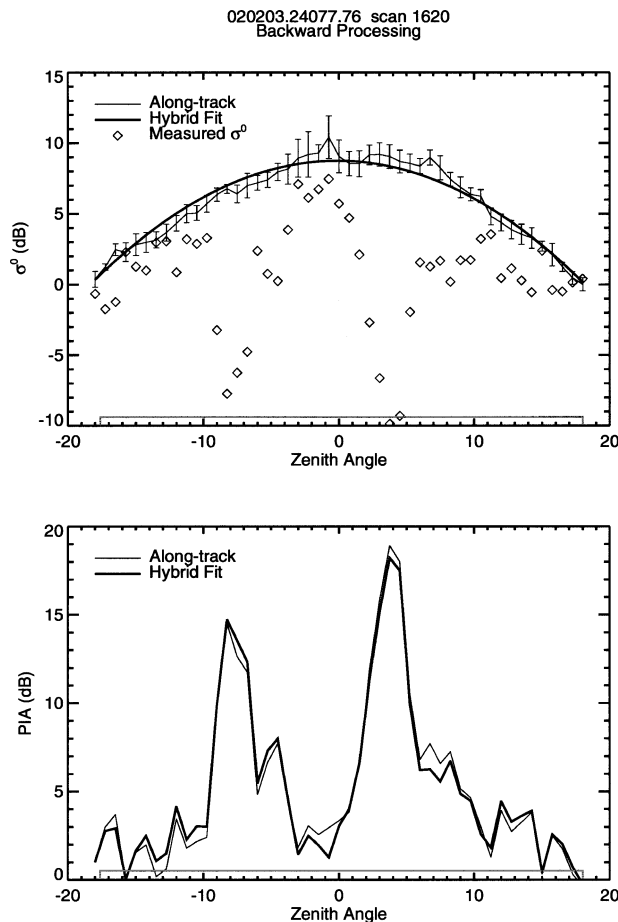


FIG. 8. Same as Fig. 7, but where the orbit is processed backward.

mates is required to be 3 or greater, then about 80% of the rain data must be excluded.

Examples of the PIA derived from the along-track and hybrid surface references were shown in Figs. 4 and 7 for the forward estimates and in Figs. 5 and 8 for the corresponding backward estimates. It is instructive to calculate δA and δA_N by replacing the hybrid with the along-track reference data. The results are shown in Fig. 12. The distributions are broader in this case than those in Fig. 11. In particular,

$$[\text{Pr}(|\delta A|) < 0.7 \text{ dB}] = 0.75,$$

$$[\text{Pr}(|\delta A|) < 1.14 \text{ dB}] = 0.9,$$

$$[\text{Pr}(|\delta A|) < 1.55 \text{ dB}] = 0.95.$$

For example, when using the along-track reference, the forward and backward estimates are within 0.7 dB of each other in 75% of the cases. In contrast, when the hybrid reference is used almost exclusively, the forward and backward estimates are within 0.46 dB of each other for the same percentage of cases. The narrower distribution of differences represents an advantage of the hybrid over the along-track reference. As noted earlier, an advantage of the hybrid over the combination of along-

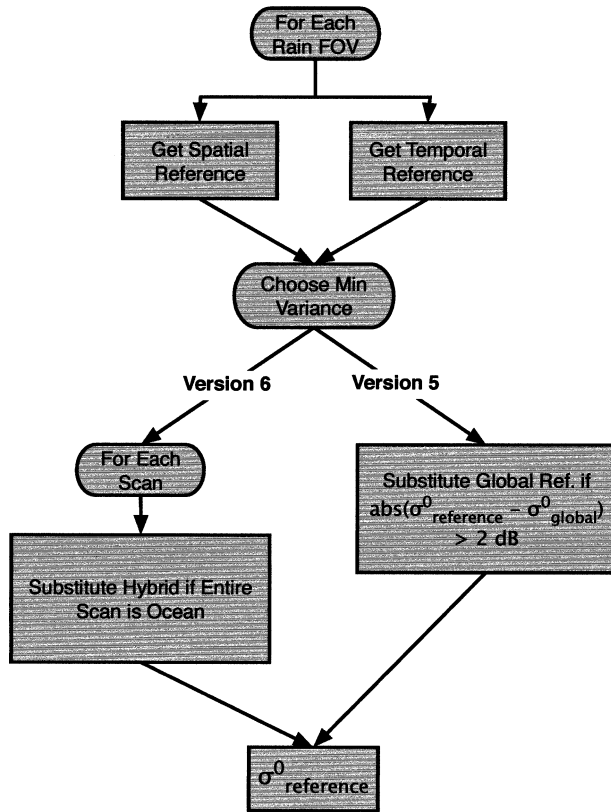


FIG. 9. Flow diagram for the selection of the surface reference value for versions 5 and 6 of the algorithm.

track, temporal, and global reference data used in version 5 of the algorithm is that discontinuities in the PIA can be greatly reduced.

c. Statistics of PIA over land

Despite the generally good results of the hybrid reference over ocean, its application over land has been unsuccessful. Over land, the angular dependence of σ^0 cannot be modeled as a quadratic. Although third- or fourth-order polynomials fit separately to data in the right- and left-hand sides of the swath are more accurate, the high variability of the surface cross section near nadir often yields reference curves that are poor representations for the cross-track rain-free data. In light of these problems, the decision was made to use the version 5 algorithm over land or over scans in which more than one background type is present. In these cases the reference dataset is selected either as the along-track spatial or temporal, depending on which has the smaller variance.

The same 2 weeks of data described above were also used to assess the SRT over land. Of the 2 270 263 raining fields of view detected over this period, 329 643, or 14.5%, occurred over land, 84.3% over ocean, and the remainder (1.2%) over coast. Of the raining pixels

over land, 150 119, or 46.5%, were classified as at least marginally reliable, that is, with a corresponding reliability that is greater than unity, for both the forward and backward processing. Because of the high variability of the land cross sections, the percentage of cases where the forward (backward) PIA estimate alone was marginally reliable was significantly higher: 63% (60%). Of the 46.5% of the marginally reliable and reliable cases, the along-track spatial is used as reference in about 90% of the cases, the temporal in 10%.

Histograms of δA and δA_N for the land cases are shown in the upper and lower panels of Fig. 13. There are several differences between this and the histogram for oceanic rain in Fig. 11. Over land, the distribution of differences between the forward and backward PIA estimates is significantly broader than that over ocean. For example, 75% of the data have absolute differences between A_F and A_B of less than about 1.5 dB, while 95% of the data have differences of less than 4 dB. As already noted, over oceans, using the hybrid reference, these differences are 0.46 and 1.12 dB, respectively, or about a factor of 3 smaller. Another feature in the results over land is the discontinuity in the histogram at $\delta A = 0$. Because the temporal reference data depend only on location and incidence angle, the reference data are the same for forward and backward processing, so that $\delta A = A_F - A_B = 0$. Because these cases do not constitute an independent estimate of the PIA we have excluded points where δA is identically zero in calculating the thresholds given above. For the histograms of the normalized difference, δA_N (Fig. 13, bottom), we find that for 75% of the data the difference in path attenuation between the forward and backward estimates is less than about 55% of the mean value, and for 90% of the data the difference is less than about 85% of the mean. If we restrict the data so that only those estimates with reliability greater than 3 are chosen, we find that 75% of the $|\delta A_N|$ are less than 0.2 and 95% of the $|\delta A_N|$ are less than 0.5. As in the case of the ocean background, this filtering eliminates a large fraction of the data. As noted earlier, 46.5% of the raining data over land have a reliability factor greater than unity for the estimates processed forward and backward. If we require the reliability factor to be greater than 3 for both forward and backward estimates then only about 8% of the raining data is retained.

5. Summary and conclusions

In the single-wavelength version of the surface reference technique, the estimate of path attenuation is taken to be the difference between a mean surface cross section measured outside the rain, the reference value, to the apparent surface cross section measured in the rain. A major issue in applying the method is what constitutes an appropriate surface reference. In an earlier operational version of the algorithm, several rain-free reference datasets were defined: the along-track spatial,

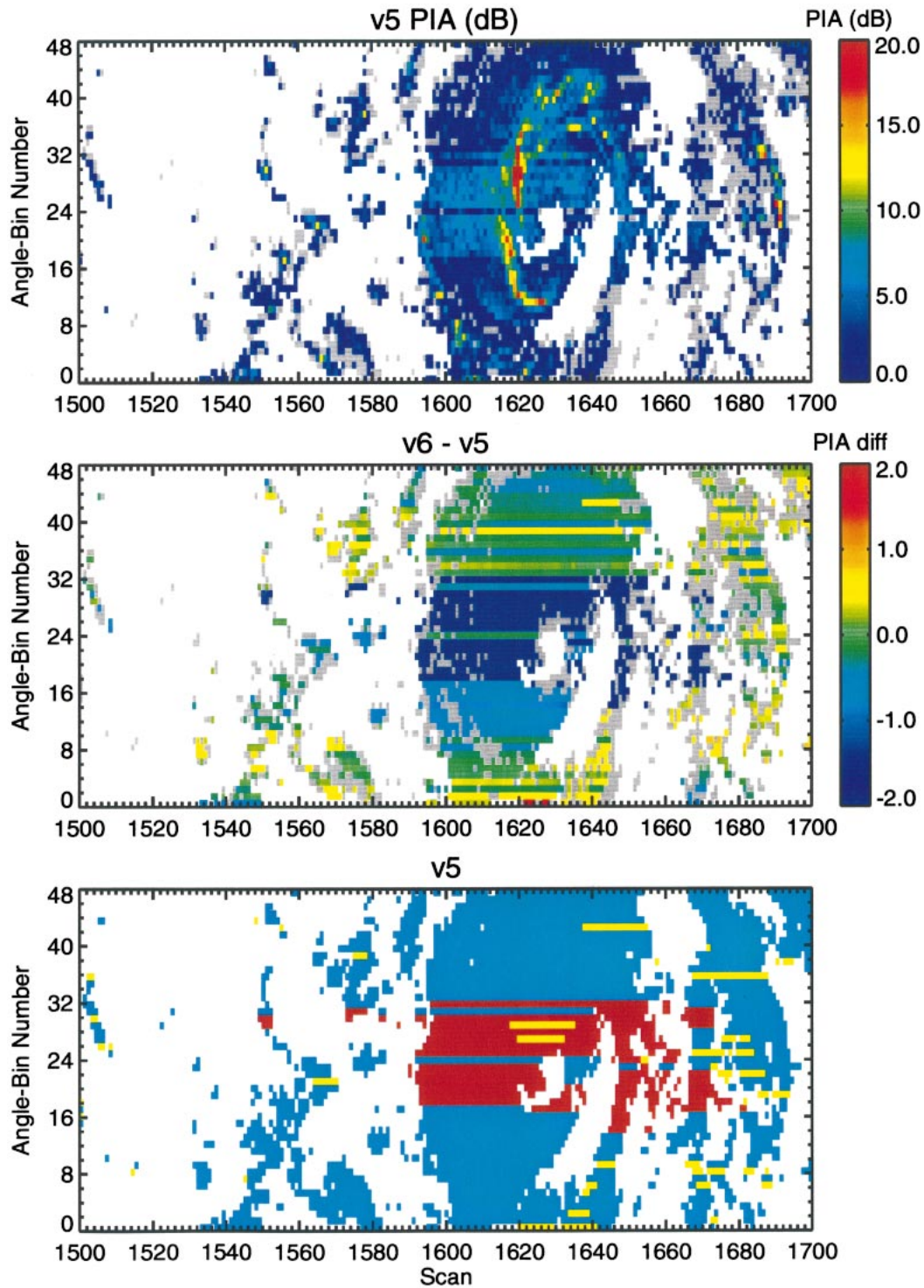


FIG. 10. (top) Estimates of two-way path-integrated attenuation using the version 5 processing algorithm (2a21). (middle) Difference between the PIA as estimated from the hybrid reference (top, Fig. 6) and the PIA shown in the top panel. (bottom) Reference datasets used in the determination of the PIA shown in the top panel. Along-track reference is used in the blue areas, temporal reference is used in the yellow areas, and global reference is used in the red areas.

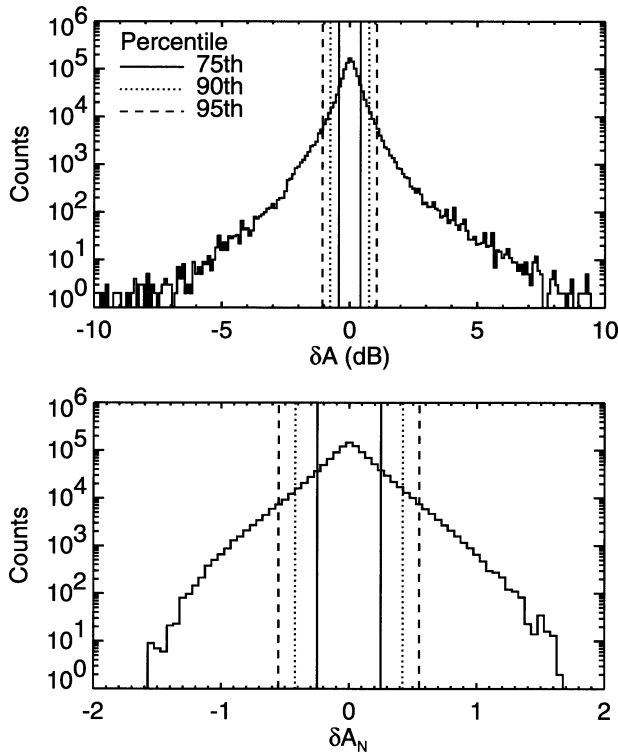


FIG. 11. (top) Histogram of the difference between the PIA estimated from forward and backward processing using primarily the hybrid reference. The region between the solid lines represents 75% of the data; the regions between the dotted and dashed lines represent, respectively, 90% and 95% of the data. (bottom) Histogram of the normalized difference in PIAs.

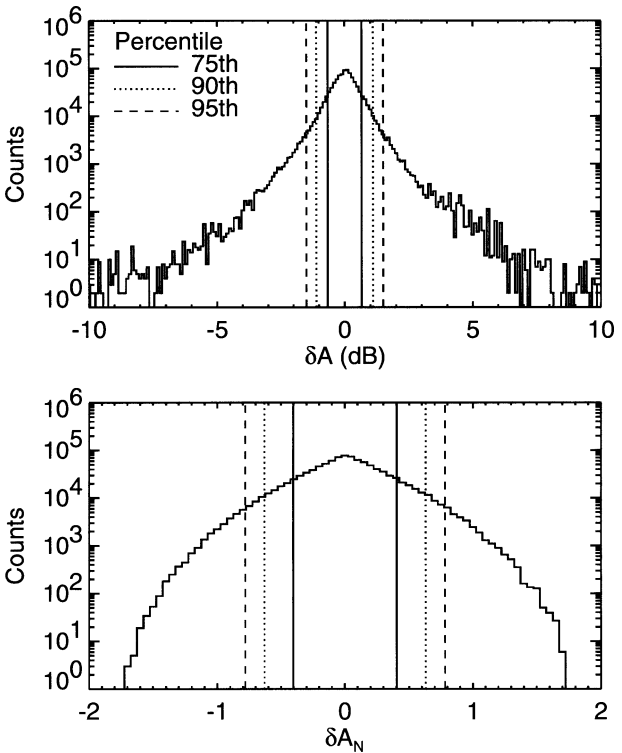


FIG. 12. Same as Fig. 11, but using the along-track reference data.

the temporal, and the global. The reference data used to compute the PIA essentially were those that had the smallest standard deviation associated with them. This criterion, however, leads in some cases to changes in the reference dataset from angle to angle, causing discontinuities in the PIA field. In addition, the along-track spatial reference itself can lead to abrupt changes in the estimated attenuation. To circumvent this type of error, a hybrid surface reference was defined over ocean that uses a combination of the along-track and cross-track data. Assessing the stability of the estimate by processing the orbits forward and backward indicates that the hybrid reference largely eliminates discontinuities in the PIA field. It also yields more consistent estimates of PIA than does the along-track reference, in the sense that the distribution of differences in path attenuations from the forward and backward processing has a smaller variance.

Further improvements in the application of the surface reference technique are desirable. The hybrid reference, in its present form, performs well only over oceans. Over land, where a combination of the along-track and temporal reference datasets continues to be used, the path-attenuation estimates are significantly less accurate. For data processed only in the forward direc-

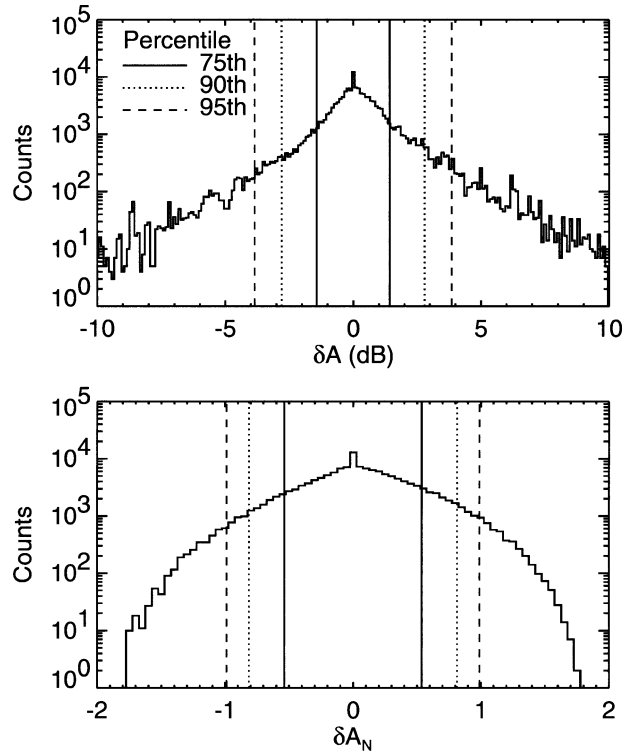


FIG. 13. Same as Fig. 11, but over land. Both along-track spatial and temporal reference datasets are used.

tion, the reference datasets at or near a land–water boundary are sometimes inappropriate, in the sense that the spatial reference data are available only at great distances from the raining area while the temporal reference, because it contains a mixture of data from land and ocean, is only marginally useful. None of the reference datasets are well suited to rain over inland water or over islands that are small or comparable in size to the PR swath (220 km). Although the inverse of the fractional standard deviation of the PIA estimate provides a useful measure of reliability, information on the self-consistency of the estimate can be gained by processing the orbits backward as well as forward. While backward processing is not planned for version 6 of the algorithm, changes to the code and to the operational environment may make it feasible in the future.

The focus of this paper is on improving the operational estimates of path attenuation from the SRT by using a more robust form of the surface reference data over ocean. Assessing the accuracy of the method relative to the Hitschfeld–Bordan and other alternatives is a topic of future study, the objective of which will be to identify a method or combination of methods that provides the most accurate estimate of path attenuation for a single-wavelength spaceborne weather radar.

REFERENCES

- Bliven, L. F., and J. P. Giovanangeli, 1993: An experimental study of microwave scattering from rain- and wind-roughened seas. *Int. J. Remote Sens.*, **14**, 855–869.
- Draper, D. W., and D. G. Long, 2002: An assessment of SeaWinds on QuikSCAT wind retrieval. *J. Geophys. Res.*, **107**, 3212, doi:10.1029/2002JC001330.
- Durden, S. L., and Z. S. Haddad, 1998: Comparison of radar rainfall retrieval algorithms in convective rain during TOGA COARE. *J. Atmos. Oceanic Technol.*, **15**, 1091–1096.
- , L. Li, and S. H. Yueh, 2003: A surface reference technique for airborne Doppler radar measurements in hurricanes. *J. Atmos. Oceanic Technol.*, **20**, 269–275.
- Freilich, M. H., and B. A. Vanhoff, 2003: The relationship between winds, surface roughness, and radar backscatter at low incidence angles from TRMM Precipitation Radar measurements. *J. Atmos. Oceanic Technol.*, **20**, 549–562.
- Hitschfeld, W., and J. Bordan, 1954: Errors inherent in the radar measurement of rainfall at attenuating wavelengths. *J. Meteor.*, **11**, 58–67.
- Iguchi, T., and R. Meneghini, 1994: Intercomparison of single-frequency methods for retrieving a vertical rain profile from airborne or spaceborne radar data. *J. Atmos. Oceanic Technol.*, **11**, 1507–1516.
- , T. Kozu, R. Meneghini, J. Awaka, and K. Okamoto, 2000: Rain profiling algorithm for the TRMM Precipitation Radar. *J. Appl. Meteor.*, **39**, 2038–2052.
- Kozu, T., and Coauthors, 2001: Development of precipitation radar onboard the Tropical Rain Measuring Mission (TRMM) satellite. *IEEE Trans. Geosci. Remote Sens.*, **39**, 102–116.
- L'Ecuyer, T. S., and G. L. Stephens, 2002: An estimation-based precipitation retrieval algorithm for attenuating radars. *J. Appl. Meteor.*, **41**, 272–285.
- Li, J., and K. Nakamura, 2002: Characteristics of the mirror image of precipitation observed by the TRMM Precipitation Radar. *J. Atmos. Oceanic Technol.*, **19**, 145–158.
- Li, L., and Coauthors, 2001: Retrieval of atmospheric attenuation using combined ground-based and airborne 95-GHz cloud radar measurements. *J. Atmos. Oceanic Technol.*, **18**, 1345–1353.
- , E. Im, S. L. Durden, and Z. S. Haddad, 2002: A surface wind model-based method to estimate rain-induced radar path attenuation over ocean. *J. Atmos. Oceanic Technol.*, **19**, 658–672.
- Liao, L., R. Meneghini, and T. Iguchi, 1999: Simulations of mirror image return of air/space-borne radar in rain and their applications in estimating path attenuation. *IEEE Trans. Geosci. Remote Sens.*, **37**, 1107–1121.
- Lungu, T., 2001: QuikSCAT science data product user's manual: Overview and geophysical data products. Version 2.2, JPL D-18053, Jet Propulsion Laboratory, Pasadena, CA, 95 pp.
- Marecal, V., T. Tani, P. Amayenc, C. Klapisz, E. Obligis, and N. Vitard, 1997: Rain relations inferred from microphysical data in TOGA COARE and their use to test a rain profiling method from radar measurement at Ku-band. *J. Appl. Meteor.*, **36**, 1629–1646.
- Marzoug, M., and P. Amayenc, 1994: A class of single- and dual-frequency algorithms for rain-rate profiling from a spaceborne radar. Part I: Principle and tests from numerical simulation. *J. Atmos. Oceanic Technol.*, **11**, 1480–1506.
- Meneghini, R., J. Eckerman, and D. Atlas, 1983: Determination of rain rate from a spaceborne radar using measurements of total attenuation. *IEEE Trans. Geosci. Remote Sens.*, **21**, 34–43.
- , J. A. Jones, and L. H. Gesell, 1987: Analysis of a dual-wavelength surface reference radar technique. *IEEE Trans. Geosci. Remote Sens.*, **25**, 456–471.
- , K. Nakamura, C. W. Ulbrich, and D. Atlas, 1989: Experimental tests of methods for the measurement of rainfall rate using an airborne dual-wavelength radar. *J. Atmos. Oceanic Technol.*, **6**, 637–651.
- , T. Iguchi, T. Kozu, L. Liao, K. Okamoto, J. A. Jones, and J. Kwiatkowski, 2000: Use of the surface reference technique for path attenuation estimates from the TRMM Precipitation Radar. *J. Appl. Meteor.*, **39**, 2053–2070.
- Quartley, G. D., M. A. Srokosz, and T. H. Guymer, 1999: Global precipitation statistics from dual-frequency TOPEX altimetry. *J. Geophys. Res.*, **104**, 31 489–31 516.
- Tian, L., G. M. Heymsfield, and R. C. Srivastava, 2002: Measurements of attenuation with airborne and ground-based radar in convective storms over land and its microphysical implications. *J. Appl. Meteor.*, **41**, 716–733.
- Walsh, E. J., C. W. Wright, D. Vandemark, L. F. Bliven, E. Ulhorn, P. G. Black, and F. D. Marks, 2002: Rain rate measurement with an airborne scanning radar altimeter. *Proc. IGARSS2002*, Vol. III, Toronto, ON, Canada, IGARSS, 1875–1876.
- Yang, Z., S. Tang, and J. Wu, 1997: An experimental study of rain effects on fine structures of wind waves. *J. Phys. Oceanogr.*, **27**, 419–430.